

TALLINN UNIVERSITY OF TECHNOLOGY

Faculty of Science

Marine Systems Institute

**MANIFESTATION OF MESOSCALE PROCESSES ON
DIFFERENT TYPE OF SATELLITE IMAGERY IN THE
BALTIC SEA**

Bachelor's thesis

Karli Spitsõn

Supervisor: PhD Rivo Uiboupin,
Chair of Oceanography,
Research Scientist

Earth Sciences
2015

I hereby declare that this bachelor's thesis is the original product of my investigation and the materials used in this dissertation have not been submitted previously to apply for a scientific degree.

I assure that all statements made by other authors and materials used in this dissertation have been properly referenced to.

Karli Spitsõn

Supervisor: Rivo Uiboupin

This bachelor's thesis fulfills the requirements presented to it.

The Chief of Defense: Accepted for defending of a bachelor's thesis

..... (Name, signature, date)

TALLINNA TEHNIKAÜLIKOOL
Matemaatika-loodusteaduskond
Meresüsteemide Instituut

**MESOMASTAAPSETE PROTSESSIDE ILMNEMINE
ERINEVAT TÜÜPI SATELLIIDIPILTIDEL
LÄÄNEMERES**
Bakalaureusetöö

Karli Spitsõn

Juhendaja: Rivo Uiboupin,
Okeanograafia õppetool,
Vanemteadur

Maa-teadused
2015

Abstract

This bachelor's thesis focuses on comparing the effects of different satellite image resolutions on the apparent manifestation of mesoscale processes in the Baltic Sea. The actuality of this topic lies in the constant growth of data computing power of today's computer chips, which allows researchers to study ocean processes in more detail and on larger scales.

During the course of this study, spectra from mesoscale processes in a common study area are correlated to see how using different image resolutions on them changes the spectra output. Two study sites are used for this purpose - the Baltic Sea proper and the Gulf of Finland, where 2D-FFT algorithm is utilized to calculate the spectra and spectral slopes of mesoscale processes found within. Images used in this study originate from 3 different satellite instruments - Thematic Mapper, MERIS and ASAR, each with a different resolution from one-another. Satellite data is obtained through various online databases where focus is put on finding common areas and dates of acquisition for two instruments at a time, which are then paired for spectra comparison. Image pairs looked at in this study are Thematic Mapper-MERIS and ASAR-MERIS.

This study concluded that while some minor correlation could be seen between different instruments, there also exist irregularities and further investigation needs to be conducted to make a more concrete statement.

Key words: Mesoscale, the Baltic Sea proper, the Gulf of Finland, satellite imagery, MERIS, Thematic Mapper, ASAR.

Lühikokkuvõte

Käesolev bakalaureusetöö uurib mesomastaapsete protsesside ilmnemist erineva lahutusvõimega satelliidipiltidel Läänemeres. Teema aktuaalsus seisneb arvutite andmetöötlusmahu pidevas kasvus, mis laseb okeanograafidel uurida üha suurema resolutsiooniga mereliste protsesside omadusi suurtel merealadel. Antud töö käigus vaadeldakse spetsiifiliselt erineva pildiresolutsiooni puhul väljastatavate spektrite korrelatsiooni. Uuringualadeks on valitud Läänemere avaosa ja Soome laht, mis kumbki iseloomustavad erinevat tüüpi veekogu. Töös kasutatakse kolme erinevat mõõtmisandurit - Thematic Mapper, MERIS ja ASAR, mille pildid saadakse läbi *online* andmebaaside, kus jälgitakse, et kahe erineva satelliidi kaupa oleks olemas pildid ühise piirkonna ja aja kohta. See on vajalik, et saaks võrrelda kõrvuti kahte eri lahutusvõimega satelliidipilti - L5TM ja MERIS ning ASAR ja MERIS. Piltidele, mida antud töös käsitletakse, rakendatakse 2D-FFT algoritmi, mille väljundiks on sageduse spektrid, kust saab omakorda arvutada piltide spektraaltõusud.

Tulemusi analüüsidest leiti erinevate instrumentide vahel mõningast korrelatsiooni, kuid tõdeti, et parema ülevaate saamiseks peab antud teemal läbi viima põhjalikuma uurimuse, kuhu on kaasatud suurem hulk satelliidipilte.

Võtmesõnad: Mesomastaap, Läänemere avaosa, Soome laht, satelliidipildid, MERIS, Thematic Mapper, ASAR.

TABLE OF CONTENTS

INTRODUCTION	1
Mesoscale and submesoscale processes	1
Remote sensing and FFT	2
Wavenumber spectra	3
Study site	4
1. OBJECTIVES	6
2. DATA	7
2.1. Instruments	7
2.2. Locations	8
3. METHODS	10
4. RESULTS	12
4.1. Case studies for different power-law slopes	19
5. DISCUSSION	21
6. SUMMARY AND CONCLUSION	23

INTRODUCTION

Mesoscale and submesoscale processes

The oceanic circulation is characterized not only by large-scale currents such as the Gulf Stream, but also by smaller, mesoscale (diameter 10–100 km; duration days-weeks) and submesoscale structures (1-10 km; duration ≤ 1 day) (León *et al*, 2014; Klein and Lapeyre, 2009; Lévy *et al*, 2012). Cyclonic and anti-cyclonic oceanic eddies are the oceanic counterpart for a weather system. They play a key role in the Ocean's ecosystem structure and dynamics (Klein and Lapeyre, 2009). Eddies are rotating vortices and their main role is to transport and mix water masses (Leppäranta and Myrberg, 2009: 152). Close to 80-90% of the Ocean's kinetic energy comes from oceanic eddies (Sasaki *et al*, 2014; Ferrari and Wunsch, 2009). It has been noted that baroclinic instability is the main force behind eddy generation mechanism, other sources being for example atmospheric forcing (Stammer, 1997).

Mesoscale and submesoscale structures are closely related due to the turbulent nature of oceanic flows, where energy is constantly transferred between smaller and larger scales (Ferrari and Wunsch, 2009). Submesoscale dynamics are shown to have a substantial effect on larger, mesoscale structures (Lévy *et al*, 2012; Sasaki *et al*, 2014). One of the most fundamental length scales in geophysical fluid dynamics is the Rossby radius:

$$R = \frac{c}{f} \quad (1)$$

where c is the characteristic wave speed and f ($2 \omega \sin\phi$) is the Coriolis parameter (Leppäranta and Myrberg, 2009: 134). It describes the horizontal scales of mesoscale processes. More precisely, Rossby radius of deformation defines the radius at which

rotational effects become as important as buoyancy. (Alenius *et al*, 2003) Pavelson (2005) has mentioned that in spite of the logical naming for different structure scales, the term ‘mesoscale’ has been often used to denote different hydrographical scales. Mesoscale eddies are usually defined in the order of the first baroclinic Rossby radius of deformation, R_1 (Osiński *et al*, 2010; Lévy *et al.*, 2001). In the Baltic Sea baroclinic (internal) R_1 is 1-10 km, whereas in the Gulf of Finland R_1 tends to be 2-4 km. It has also been noted that smaller R_1 values appear in shallow areas while bigger R_1 values are found in deeper water. (Alenius *et al.*, 2003)

Remote sensing and FFT

Spiral eddies were first discovered in Earth’s oceans about 45 years ago during the Apollo missions. Since then, numerous satellites have been sent up to investigate them more closely. (Munk *et al*, 2000) Some of the more common uses for satellite imagery are collecting information about sea surface temperature, chlorophyll a concentrations and sea level altitudes. In addition to observing Earth’s oceans through remote sensing, ocean circulation models and *in situ* measurements are also used. Satellite data provides reasonably high space–time resolution but only for the surface layer and for only a handful of biological properties. *In situ* data on the other hand provides very precise data about the ocean but is comparatively sparse. (Doney *et al*, 2009) While 3D ocean circulation models can produce quite detailed and large-scale datasets, they are still often unreliable due to uncertainties in the input values (Friedrichs *et al*, 2009).

In order to characterize and compare mesoscale processes in this study, a variant of the Fourier Transform was used. The principle of the Fourier transform, which dates back to the 19th century, is that any signal, such as a sound recording, can be represented as the sum of a collection of sine and cosine waves with different frequencies and amplitudes (Anderson, 2012). The Fast Fourier transform (FFT) algorithm together with its many successful applications represents one of the most important advancements in scientific and engineering computing in this century. It is

a fast algorithm for computing the discrete Fourier transform (DFT) where raw data on a scale of 2^n is divided into two or more subsets of smaller size and a boundary is applied to stop calculating when the datasets get small enough. (Chu and George, 2000: Preface, Chapter 3) This is a significant step forward in speeding up the Fourier transform as it reduces the calculation complexity from N^2 to $N \log_2 N$, where N is the problem size (Duhamel and Vetterli, 1990). FFT equations are derived from DFT, which is expressed as:

$$X_\gamma = \frac{1}{2n+1} \sum_{l=0}^{N-1} x_l \omega^{-\gamma l}, \quad \gamma = 0, 1, \dots, 2n \quad (2)$$

where N is equal to $2n+1$, l is length and x is a function of $f(\theta)$. Applications however often require multiple sets of one-dimensional FFTs, which has created the need to further develop the FFT algorithm to better accommodate two-dimensional calculations. The equation of a 2D-DFT is expressed as:

$$X_{\gamma_1, \gamma_2} = \sum_{l_1=0}^{N_1-1} \sum_{l_2=0}^{N_2-1} x_{l_1, l_2} \omega_{N_1}^{\gamma_1 l_1} \omega_{N_2}^{\gamma_2 l_2}, \quad (3)$$

for $\gamma_1 = 0, 1, \dots, N_1-1$, and $\gamma_2 = 0, 1, \dots, N_2-1$.

where $N_1 \times N_2$ values are stored in a matrix x and entries in the matrix are denoted by x_{l_1, l_2} . (Chu and George, 2000: Chapter 1, Chapter 23)

Wavenumber spectra

Among other parameters phytoplankton can be observed from satellite images. Phytoplankton and water vorticity share a strong anticorrelative similarity in their spacial distribution, where maximum phytoplankton concentration values correspond to minimal vorticity values and vice versa. The wavenumber spectrum of any dynamical quantity in the upper oceanic layers is known to be characterized by a value k^{-n} , with n being the spectral slope and k a certain wavenumber. The value n characterizes the spatial distribution of the quantity examined since it indicates whether the small-

scale structures are energetic (small n) or not (large n) relative to the structures of larger scales. (Lévy and Klein, 2004)

Observational studies have revealed a spatial distribution of phytoplankton in mesoscale as characterized by a wavenumber spectrum ranging from k^{-1} to k^{-3} . This strong spectral variability can be due to either the physics and/ or the biology of the observed water body. (Lévy and Klein, 2004) According to Abraham *et al* (2000), the main force influencing the growth of a phytoplankton population is the stirring motion provided by ocean movements (baroclinic instability).

Quasi-geostrophic (QG) theory describes the evolution of departures from solid-body rotation in a rapidly rotating, stably stratified fluid (Eld *et al*, 1995). Surface Quasi-Geostrophic (SQG) theory takes into account also a non-zero surface density and assumes a uniform potential vorticity in the interior. The consequence is that its three-dimensional dynamics (and in particular the vertical structure of the surface fronts) are entirely driven by the non-zero surface density. (Klein *et al*, 2008) When FFT is applied to mesoscale eddies we can see certain power-law slopes becoming dominant. For the QG theory the power-law slope is -3 according to Charney (1971), the SQG theory predicts a power-law slope of -5/3 (Klein *et al*, 2008) and high-resolution simulations and frontogenesis dictate a power-law slope of -2 (Capet *et al*, 2008a; Capet *et al*, 2008b). A study by Le Traon *et al* (2008) found that at depths smaller than 300 m and horizontal scales smaller than 300 km, the SQG theory is a much better dynamical framework for describing the ocean surface dynamics than QG theory.

Study site

The Baltic Sea is a unique basin of the World Ocean. It is small and shallow and is connected to the main Atlantic Ocean only via the Danish Straits. The exchange of water through these straits is quite limited and as a consequence of the positive freshwater balance the Baltic Sea water mass is brackish. (Leppäranta and Myrberg, 2009: 1) It has a complicated shoreline and bottom topography, and its water column

is highly stratified (Osiński *et al*, 2010). It has a mean depth of only 54 m and mean salinity of 7 ‰. A fundamental feature of The Baltic Sea is its permanent saline stratification, which limits vertical convection and consequently oxygenation of deep-water masses is weak and anoxic bottom areas are found. (Leppäranta and Myrberg, 2009: 3, 4) Two of its major basins, namely the Gulf of Finland and the Baltic Sea proper are observed more closely in this dissertation. Over half of the Baltic Sea water mass is made up of the Baltic Sea proper, which consists of the Gotland Sea, Arkona Basin and Bormholm Basin (Leppäranta and Myrberg, 2009: 15). A number of case studies based on the measurements of currents have shown that the response of the Baltic Sea is baroclinic to wind events with a duration more than 50 hours, whereas in short-term wind events (duration 10-40 hours) the response is barotropic and response to wind events shorter than 10 hours quickly vanishes. There is one order of magnitude more energy in the baroclinic mode than in the barotropic mode. Therefore, the Baltic Sea cannot be treated as a homogenous water body. (Leppäranta and Myrberg, 2009: 134) This means that it is essential to include the Baltic Sea proper alongside other study sites if any characterization of the whole Baltic Sea is to be made.

For the purpose of this study, the Gulf of Finland was chosen to represent the smaller and less saline areas of the Baltic Sea and the Baltic Sea proper to represent a more open type of brackish water body. As previously mentioned, the Baltic Sea is not a homogenous basin and as such the characteristics of its eddies must be examined if we wish to get a clear understanding of the distribution of mesoscale processes in the study area. To achieve this, two study sites with differing water properties were chosen. Different studies (Lévy and Klein, 2004; Qazi *et al*, 2014; Le Traom *et al*, 2009; Charney 1971; Stammer, 1997; Lévy *et al*, 2012; Klein *et al*, 2007; *etc...*) have shown that water parameters produce a negative spectral slope and by observing a study site at various pixel resolutions, different spectral slopes emerge (Capet *et al*, 2008a; Lévy *et al*, 2012).

1. OBJECTIVES

The goal of this study was to characterize mesoscale processes in the Baltic Sea through the use of satellite imagery in different resolutions. This was achieved by using 2D-FFT algorithm to find the spectral slopes for mesoscale processes in the Baltic Sea. These spectral slopes could then be correlated, giving an overview of how different satellite image resolutions change the spectra shapes and slopes for the Baltic Sea.

2. DATA

2.1. Instruments

Level 1 products from three different satellite instruments were used in the course of this study. First is the MEdium Resolution Imaging Spectrometer (MERIS). MERIS was a programmable, medium-spectral resolution, imaging spectrometer operating in the solar reflective spectral range (390 nm to 1040 nm). The instrument scanned the Earth's surface using the 'push broom' method over a field of view of 68.5° equivalent to 1150 km, in 15 programmable spectral bands. The field of view was shared between five identical cameras arranged in a fan shape configuration at two spatial resolutions, 300 m and 1,2 km at nadir. MERIS was a part of the ENVISAT satellite that was operated by the European Space Agency from March 2002 to April 2012, following the unexpected loss of contact with the satellite (What is Envisat? 2015). ENVISAT's orbit was ~ 800 km (Soussi, 2011). For the purpose of this dissertation, MERIS spectral band 5 was used (~ 560 nm, 300 m pixel resolution) to observe eddy vorticities through biological properties.

The second instrument is the Advanced Synthetic Aperture Radar (ASAR), which was also located on the ENVISAT satellite (Instruments, 2015). ASAR was a high resolution imaging radar with a pixel resolution ranging from 75 to 1000 m. It could be operated in 5 distinct measurement modes: Image Mode (IM), Alternating Polarization Mode (AP), Wide Swath Mode (WS), Global Monitoring Mode (GM), and Wave Mode (WV). (Kult, 2015: 19, 80) WS mode products are used in this dissertation, which had a resolution of 75 m and a wavelength of 5,6 cm (Design, 2015).

The third instrument is the Landsat-5 Thematic Mapper (L5TM), which was sent up into orbit in March 1984 on the LANDSAT-5 satellite. The Thematic Mapper instrument stopped working in November 2011 whereas the LANDSAT-5 satellite as a whole stopped working in January 2013. (Landsat 5 History, 2015) L5's orbit was 705 km and its TM instrument had seven spectral bands: six 30 m reflective bands and one 120 m thermal band. TM bands have center wavelengths of 490, 560, 660, 830, 1670, 1150, and 2240 nm, respectively (Barsi *et al*, 2007; Chander *et al*, 2007). TM images have a swath of 185 km (The Thematic Mapper, 2015). TM Band 2 products (520- 600 nm, 30 m pixel resolution) were used in this dissertation.

2.2. Locations

Study sites were chosen in such a way that they would cover most of the two basins. In each case MERIS image was paired with an ASAR or L5TM image, where both images were acquired within 24 h. Major limitations in choosing suitable data for this study were the presence of cloud cover and the number of satellite pictures available. As a result the total number of satellite images used for L5TM-MERIS was 12, out of which 35 smaller scenes were cut as 1024x1024 and 2048x2048 pixel size scenes (see *fig. 1*). For ASAR-MERIS a total of 11 satellite images were used, out of which 16 scenes with scene sizes of 1024x1024 and 2048x2048 were cut (see *fig. 2*). For L5TM-MERIS 15 image pairs were taken from the Gulf of Finland and for ASAR-MERIS 1 pair from the Gulf of Riga. All of the remaining pairs from both L5TM and ASAR were situated in the Baltic Sea proper. Radiance data was provided by L5TM and MERIS images while ASAR images contained raw backscatter data (amplitude).

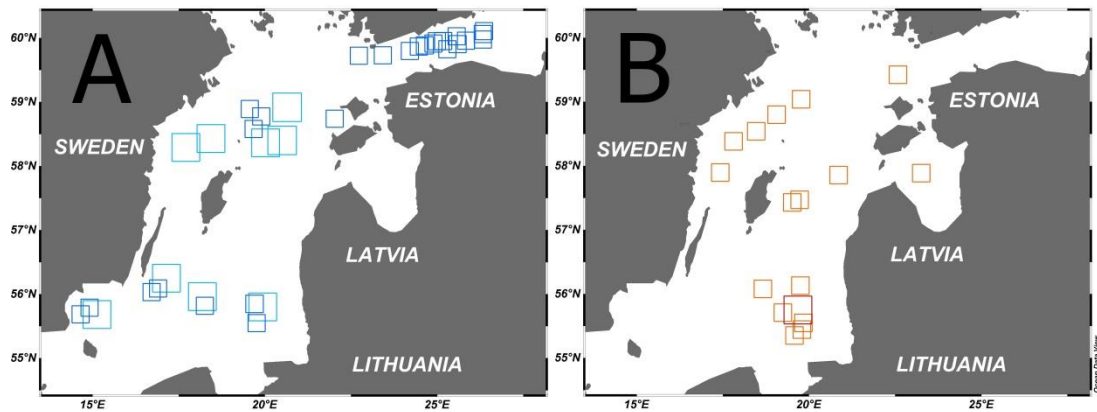


Fig. 1. In the picture 'A' locations for L5TM-MERIS image pairs in the Baltic Sea proper and the Gulf of Finland are shown. Teal squares represent 2048x2048 pixel scenes while blue squares represent 1024x1024 pixel scenes. In the picture 'B' locations for ASAR-MERIS image pairs for the Baltic Sea proper can be seen. Red square represents a 2048x2048 pixel scene and orange squares represent 1024x1024 pixel scenes.

3. METHODS

The data processing chain is shown in *fig. 2* as a flowchart. Each step is described in detail as follows.

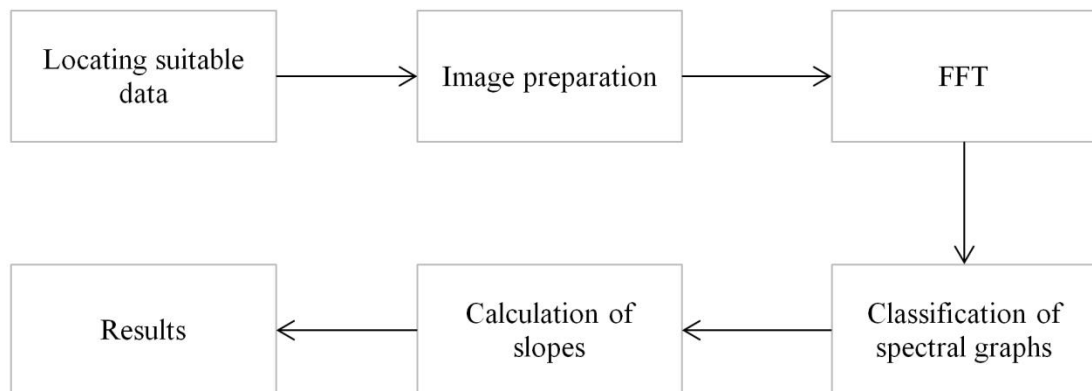


Fig. 2. Data processing flowchart.

As a first step suitable satellite imagery was located. L5TM images were obtained from Earthexplorer at the USGS website, MERIS images from Calvalus portal at Coastcolour website and ASAR images through G-POD service at ESA website. Potential images was filtered out based on the availability of L5TM and ASAR images, as they were to be used as master files while MERIS images were to be used as slave files for resampling purposes. L5TM-MERIS and ASAR-MERIS pairs were considered acceptable if they both covered a common area of at least 1024x1024 pixels and were acquired within 24 h of each other. For L5TM-MERIS pairs 1024x1024 pixel scenes covered an area of 30,72 km and 2048x2048 pixel scenes an area of 61,44 km. ASAR-MERIS covered an area of 76,8 km for 1024x1024 pixel scenes and 153,6 km for 2048x2048 pixel scenes. All of the 35 L5TM-MERIS image pairs were obtained from July-August blooms while 4 out of 16 ASAR-MERIS

image pairs depicted April-May blooms and the remaining 12 depicted July-August blooms. After gathering enough L1 (partially pre-processed images) image pairs, they were moved into the satellite processing program BEAM. For L5TM's 'band_2' images Band Math was used to turn raw pixel data into radiance values.

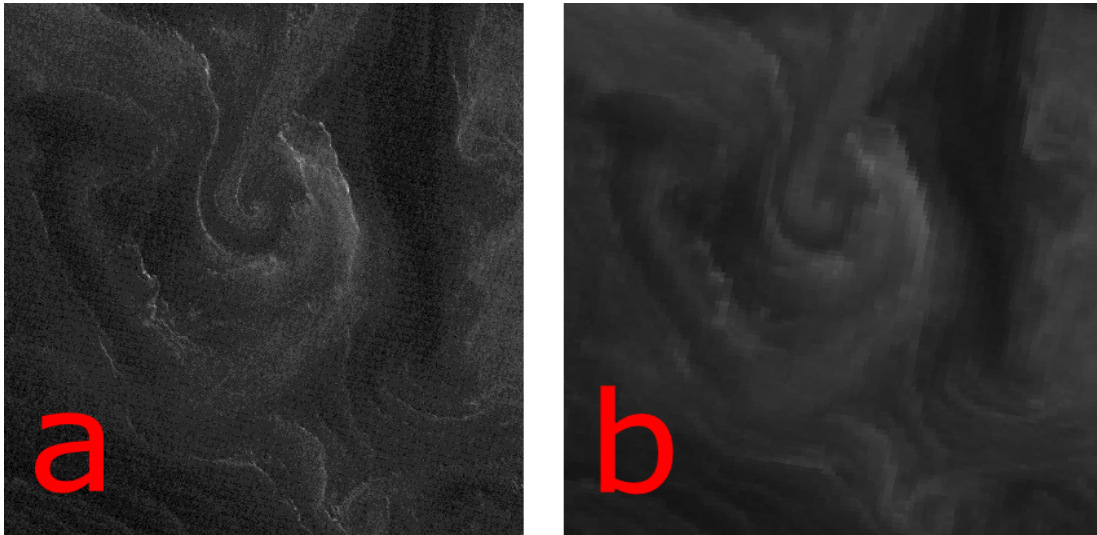


Fig. 3. Shown in the picture 'a' is an eddy from an L5TM image taken near Stockholm, Sweden on 08.08.2009 and on the picture 'b' is the matching MERIS image. L5TM's 30 m resolution describes the physical properties of an eddy more clearly than MERIS' 300 m resolution.

Then Collocation was applied to align and resample slave files onto the master grid, giving L5TM-MERIS pairs a resolution of 30 m through resampling and for ASAR-MERIS a resolution of 75 m. Different TIFF files with scene pixel sizes of 1024x1024 and 2048x2048 were created , after which the TIFF files were taken to the math program IDL, where 2D-FFT for both master and slave bands was calculated. IDL output data was then moved into Microsoft Excel where the data was processed further to make log-log plots look clearer and easier to comprehend. Finally the spectral slopes were calculated, which led to the *Results* section of this study where slopes could be examined and categorized in detail.

4. RESULTS

Spectral slopes for the data used in this study were calculated in three wavenumber ranges where a clear slope was visible. This was due to the second part of some spectra differing noticeably from the latter part. For MERIS images the slopes were calculated between $k = 0,1 - 1$ (or 10 km to 1 km), L5TM between 0,1 - 1 and 1 - 10 and ASAR between 0,1 - 1 and 1 - 8. Comparing FFT spectra and spectral slopes for each instrument at wavenumbers 0,1 - 1 showed that L5TM (30 m resolution) produced the flattest spectral slopes, followed closely by ASAR (75 m resolution) and thirdly MERIS (300 m resolution), which had the steepest spectral slope (*fig. 4*). These results support the findings of Lévy *et al* (2012) where it was found that bigger grid resolutions for a model produce flatter spectral slopes. While the radiance data for L5TM and MERIS and amplitude data for ASAR each had an easily distinguishable spectral slope, they varied greatly on the vertical axis. L5TM average radiance spectra energy values varied as much as 500 times, MERIS average values up to 100000 times and for ASAR the average amplitude values varied 100 times. Even though the values for each instrument varied greatly on the vertical axis, the actual spectra shapes rarely differed from one-another, as can be seen on *fig.4* and *fig. 5*. Biggest spectra shape differences were seen for L5TM (*fig. 5A*), where L5TM was split into two groups: L5TM flat and L5TM steep and also on MERIS(ASAR) graph (*fig. 5D*). This division was only applied to L5TM data as in the case of ASAR and MERIS images the spectra shapes did not differ noticeably on a log-log plot.

In order to determine the conditions for when different scenes produced either maximal or minimal spectral slope values the spectral slopes were lined up with their

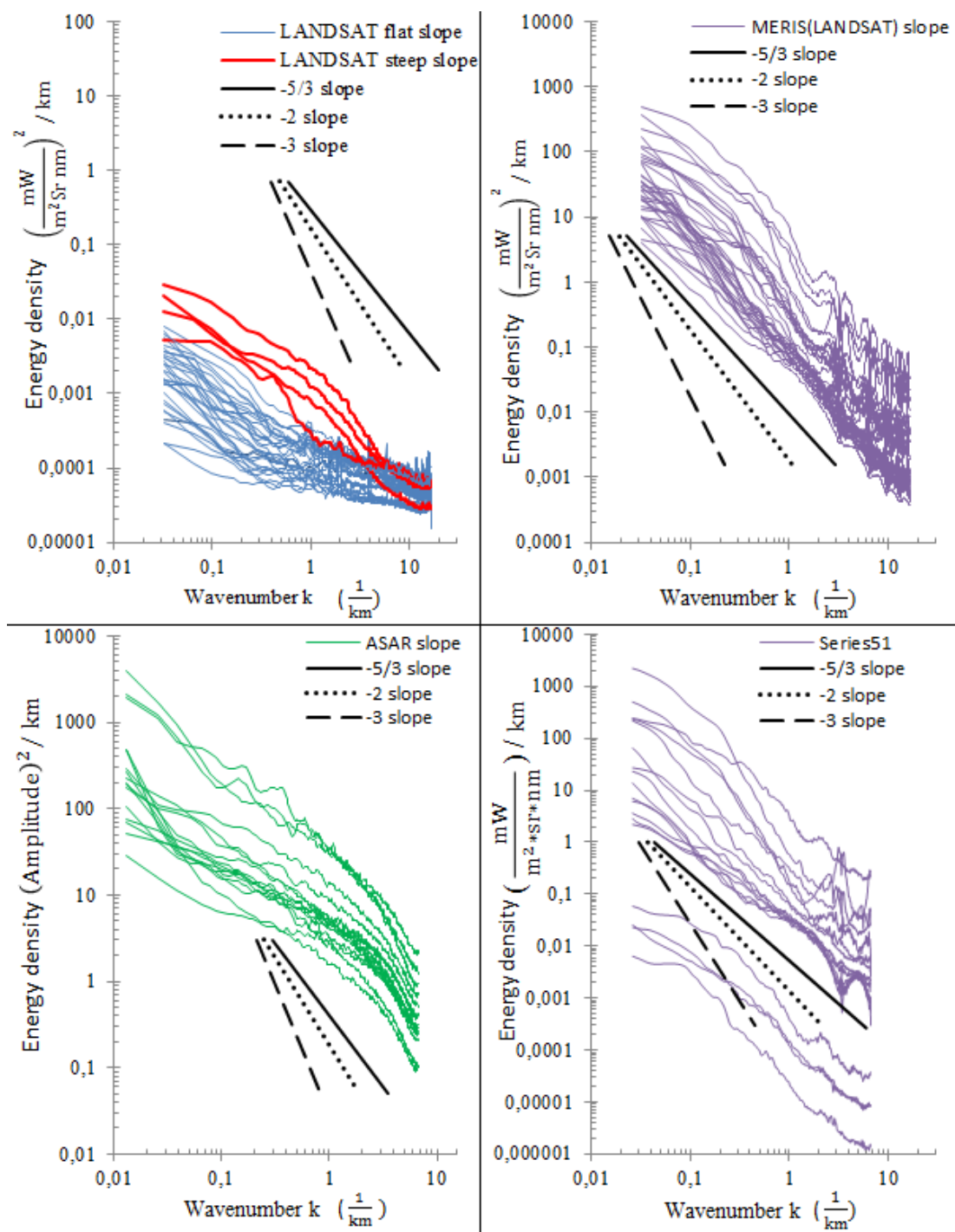


Fig. 4. Graph A shows L5TM flat and steep spectra, graph B shows MERIS (paired with L5TM) spectra, graph C shows ASAR spectra and graph D shows MERIS (paired with ASAR) spectra. On each graph are also added three power-law slopes as dictated by different spectral slope theories.

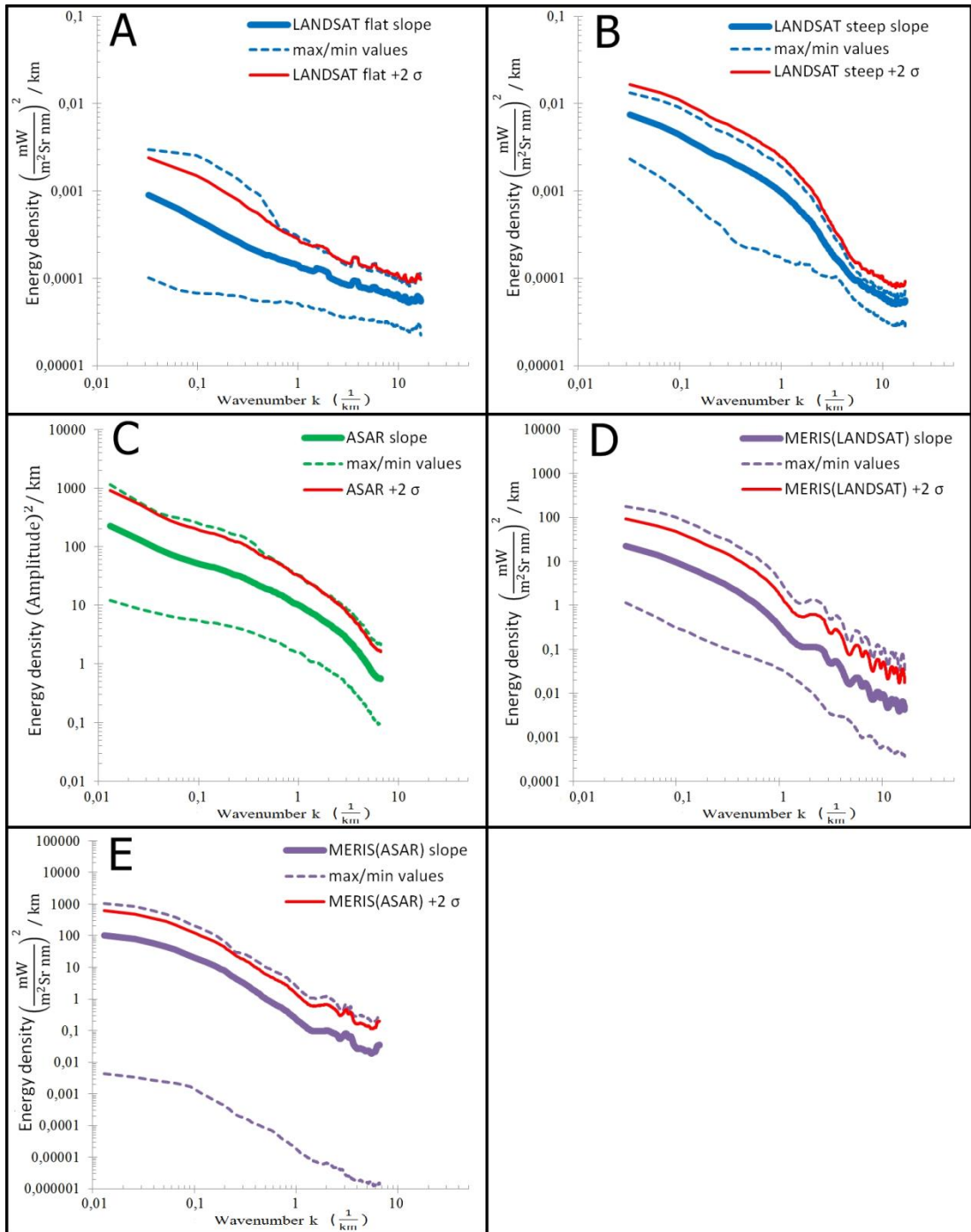


Fig. 5. Shown above are the mean slopes for each of the instruments including their corresponding max and min values and +2 st. dev. Graph A shows the mean slope for all flat L5TM spectra, graph B shows the mean slope for all steep L5TM graph C shows the mean slope for all ASAR spectra, graph D shows the mean slope for all MERIS spectra which were paired with L5TM images and graph E shows the mean slope for all MERIS spectra which were paired with ASAR.

corresponding satellite images. In the wavenumber range 0,1 - 1 L5TM and MERIS(L5TM) showed maximal slope values when no small-scale processes were present on the scenes (*fig. 6*). For MERIS(L5TM) there was very little difference in the characteristics of both max and min slope values (*fig. 7*) which made them fairly indistinguishable from each other based only on visual cues of the satellite images. This irregularity was present on numerous MERIS scenes. L5TM minimal spectral slopes appeared when there were little to no submesoscale vorticity lines present on the scenes.

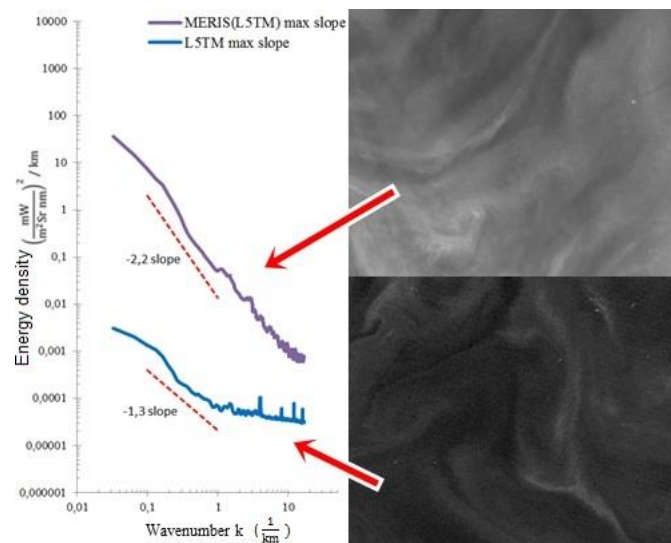


Fig. 6. Graph shows L5TM and MERIS(L5TM) maximum spectral slope and their corresponding satellite images. MERIS(L5TM) (on top) was taken on 9.07.2003 west from Saaremaa and L5TM image (bottom) was taken on 8.08.2009 east from Öland.

ASAR produced maximal spectral slopes when the scenes were dominated by mesoscale and submesoscale eddies (*fig. 8*), whereas minimal slopes were seen when a portion of the scene was rather inactive (*fig. 9*). MERIS(ASAR) scenes produced maximal slopes when there were only a few submesoscale vorticity lines present (*fig. 8*) and minimal slopes when submesoscale vorticity lines were more abundant (*fig. 9*). Cloud cover was kept on a few MERIS(ASAR) scenes to observe their effect on the spectral shapes and slopes. By comparing different images with cloud cover to their spectra it was noticed that their spectra had an outward curved shape in the

wavenumber region 0,1 - 0,5 (*fig. 8 and fig. 9*). Such images were not used for MERIS(L5TM).

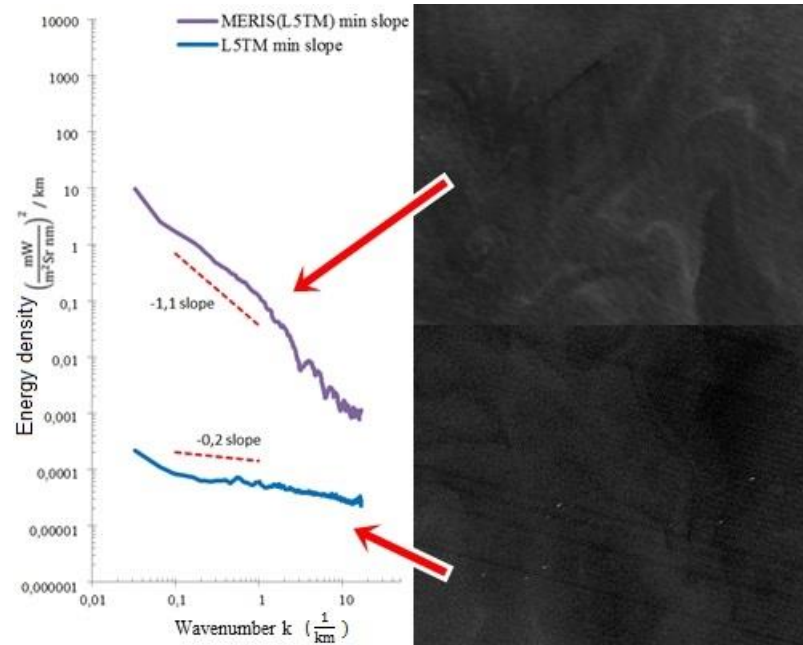


Fig. 7. Graph shows L5TM and MERIS(L5TM) minimum spectra and their corresponding satellite images. MERIS(L5TM) (on top) was taken on 4.08.2010 off the coast of Poland and L5TM (bottom) was taken on 20.08.2005 near Bornholm.

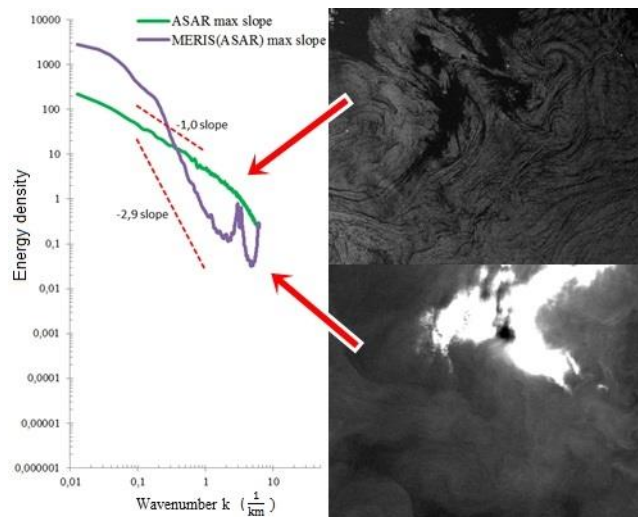


Fig. 8. Graph shows ASAR and MERIS(ASAR) maximum spectra and their corresponding satellite images. ASAR image (on top) was taken on 23.07.2008 east of Stockholm and MERIS(ASAR) image was taken on 25.04.2009 off the coast of Lithuania.

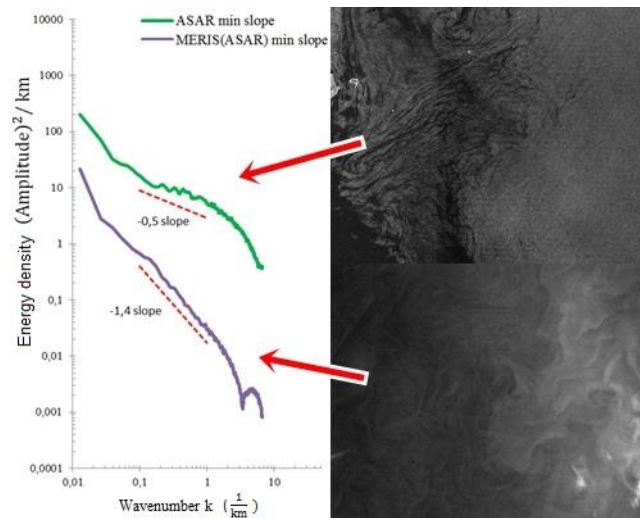


Fig. 9. Graph shows ASAR and MERIS(ASAR) minimal spectra and their corresponding satellite images. Both ASAR image (on top) and MERIS(ASAR) (bottom) were taken off the coast of Lithuania on 01.08.2008 and 25.04.2009 respectively.

In wavenumber range 1 - 6 ASAR produced maximal spectral slopes if there were numerous mesoscale vorticity lines visible (*fig. 10*) and minimal slopes when almost no activity was recorded on the satellite images (*fig. 11*). In wavenumber range 1 - 10 L5TM produced maximal slopes when there were a lot of mesoscale vorticity lines visible (*fig. 10*) and minimal slopes when there were none (*fig. 11*).

In the Baltic Sea proper basin the spectral slopes for wavenumber 0,1 - 1 showed a wide range of values for most instruments as can be seen on *Table 1*: MERIS(ASAR), MERIS(ASAR) and L5TM flat spectral slopes varied the most, by a value of 1,1. Next came ASAR (0,5) and finally L5TM steep (0,2). Possible explanations for these discrepancies are examined in the *Discussion* section of this study. In the wavenumber range 1 – 6 ASAR slope varied by 0,2 and in wavenumber range 1 – 10 MERIS steep slopes varied by 0,7.

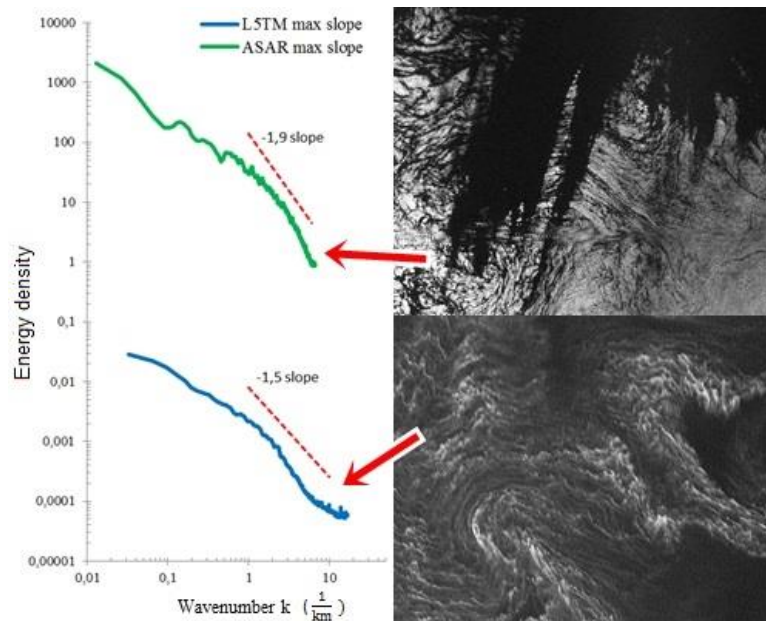


Fig. 10. Graph shows ASAR and L5TM maximum spectra, slopes and their corresponding satellite images. ASAR image (on top) was taken on 06.08.2009 near Stockholm and L5TM image (bottom) was taken on 21.07.2010 off the coast of Lithuania.

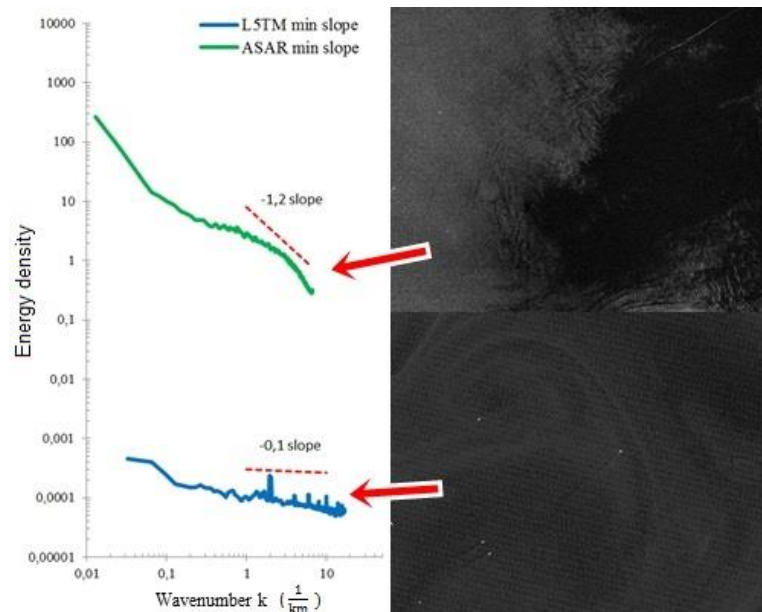


Fig. 11. Graph shows ASAR and L5TM minimum spectra, slopes and their corresponding satellite images. ASAR image (on top) was taken on 23.07.2009 off the coast of Lithuania and L5TM (bottom) was taken on 08.08.2009 east of Öland.

Table 1

Mean spectral slopes in the Baltic Sea proper basin for each instrument ($k = 0,1$ to 1 ; 1 to 6 ; 1 to 10)

Instrument \ Slope	L5TM flat (0,1 to 1)	L5TM steep (0,1 to 1)	MERIS (L5TM) (0,1 to 1)	ASAR (0,1 to 1)	MERIS (ASAR) (0,1 to 1)	L5TM flat (1 to 10)	L5TM steep (1 to 10)	ASAR (1 to 6)
Mean	-0,6	-0,8	-1,7	-0,7	-1,8	-0,4	-1,4	-1,5
Min	-0,2	-0,7	-1,1	-0,5	-1,4	-0,1	-1,3	-1,2
Max	-1,3	-0,9	-2,2	-1,0	-2,9	-0,7	-1,5	-1,9
№. of images	17	3	20	15	15	17	3	15

In the Gulf of Finland basin the spectral slopes for wavenumber $0,1 - 1$ showed a similar tendency, where the mean spectral slopes for L5TM and MERIS(L5TM) both varied by $1,0$ (Table 2). Only one L5TM steep image was located in the Gulf of Finland basin due to which it was impossible to make statistics for spectra of this type. In wavenumber range $1 - 10$ L5TM flat spectral slopes varied by $0,7$.

Table 2

Mean spectral slopes in the Gulf of Finland basin for each instrument ($k = 0,1$ to 1 ; 1 to 10).

Instrument \ Slope	L5TM flat (0,1 to 1)	L5TM steep (0,1 to 1)	MERIS(L5TM) (0,1 to 1)	L5TM flat (1 to 10)	L5TM steep (1 to 10)
Mean	-0,7	-1,2	-1,7	-0,4	-0,6
Min	-0,2	-	-1,1	-0,1	-
Max	-1,2	-	-2,1	-0,8	-
№. of images	14	1	15	14	1

4.1. Case studies for different power-law slopes

To see how the current study data compared with different power-law slope theories, 3 slopes were used: $-5/3$, -2 and -3 . For wavenumber range $0,1 - 1$ MERIS(L5TM) scenes produced a mean slope of $-1,7$ which is close to $-5/3$ as dictated by the SQG theory. 15 out of 35 MERIS(L5TM) scenes produced a slope of $-1,7 \pm 0,1$ while 11/35 scenes produced a slope steeper than $-1,8$ and 9/35 scenes produced a slope flatter than $-1,6$. Spectral slope $-2 \pm 0,1$ was present on 10/35, which describes a power-law slope of -2 as dictated by the high-resolution simulation and frontogenesis

theory. The steepest slope for MERIS(L5TM) was $-2,2$, which can be seen on *fig. 6*. In the Baltic Sea proper the spectral slopes tended to be more concentrated near the average, where slopes flatter than $-1,6$ occurred 5 times out of 20, slopes between $-1,6$ and $-1,8$ 10/20 and slopes steeper than $-1,8$ 5/20. For the Gulf of Finland basin slopes flatter than $-1,6$ accounted for 4/15, slopes between $-1,6$ and $-1,8$ 5/15 and slopes steeper than $-1,8$ 6/15.

MERIS(ASAR) scenes produced a mean slope of $-1,8$, which is also close to the power-law slope $-5/3$. 3 out of 15 MERIS(ASAR) scenes produced a slope of $-1,7 \pm 0,1$, while 6/15 scenes produced a slope steeper than $-1,8$ and 6/15 scenes produced a slope flatter than $-1,6$.

For L5TM and ASAR scenes none of the spectral slopes matched the predicted power-law slopes in wavenumber range $0,1 - 1$. In the wavenumber ranges $1 - 10$ and $1 - 6$ both L5TM steep and ASAR produced a slope that was up to 2 times steeper than in wavenumber range $0,1 - 1$ in the Baltic Sea proper basin. For L5TM steep the spectral slopes did not reach $-5/3$ even once, while for ASAR spectra 6 out of 15 produced a slope close to $-5/3$ and 1 spectra even produced a slope of $-1,9$ (seen on *fig. 10*), resembling a power-law slope of -2 .

5. DISCUSSION

This study was conducted on the premise that two satellite images taken on the same date and place from a different instrument should produce similar spectral shape features. Minimum and maximum values for none of the spectra were found on the same dates. Such lack of correlation could be explained by the wavelength differences at which the instruments operated in. L5TM and MERIS operated in nm scale, whereas ASAR operated in cm scale. By changing the wavelength scale, different water processes emerge, where the spectra are not necessarily correlative among each other. This would explain the different cases where mesoscale eddies on MERIS images rarely resembled their paired ASAR and L5TM images. It was also noted that ASAR and MERIS images contained a large amount of different pixel values (high sensitivity) whereas LANDSAT contained on average <10 different values per scene (low sensitivity).

Next, L5TM-MERIS and ASAR-MERIS pairs were compared to see if they shared any common features in the spectra shapes and values. A most notable feature of L5TM and the two MERIS spectra is that at certain wavenumbers there exist strong value spikes, which are present on most of the spectra and are located at different wavenumbers for each instrument. It is difficult to assign an exact wavenumber value to where each instrument started picking up random noise and where it was a true value spike as there were indications for both explanations found. Over half of the MERIS images showed a sharp change in their spectra starting from wavenumber ~ 3 , which would indicate either a very specific biological phenomena at smaller wavelengths or just background noise created by the recording instrument ($\lambda_{k=3} \sim 300$ m, the original resolution of MERIS). Similarly, L5TM had very specific

and energetic spikes at certain intervals on their spectra, which could be explained by the instruments background noise (visible on *fig. 4B, 4D and 5A*). These spikes were not present on any of the ASAR spectra nor original images. Besides local energy value spikes there were also a large number of different average energy value spectra, where the value scales differed up to 10^6 times. This noticeable energy scale fluctuation on log-log plot was partly caused by the 2D-FFT algorithm, where scene energy values were averaged over the whole image, which in turn lowered the mean energy if there were regions of low pixel values on the scenes. The second cause was possibly the high sensitivity of MERIS and ASAR instruments, where log-log plot revealed the intensity of different mesoscale processes quite well.

Three out of the four L5TM steep spectral slopes were located on a single original L5TM image, which was taken on 21.07.2010 near the coast of Lithuania. The fourth and final semi-steep spectrum was taken on 08.07.2011 in the Gulf of Finland. When comparing these spectra and their corresponding images to all of the other L5TM satellite imagery, it was noticed that a study site with sharper, more numerous and more energetic eddies produced a more linear and steep spectral slope (see *fig. 10*). The main reason for having only two satellite images with near-perfect characteristics in this study was due to the limitations in the number of cloud-free and available images.

Out of 50 MERIS scenes 18 showed a strong resemblance to a power-law slope of $-5/3$ and 16 scenes a power-law slope of -2 . This correlation with different power-law slopes was also noticed with ASAR, where 6 spectra out of 15 produced a slope close to a power-law slope of $-5/3$ and one slope close to -2 . Such power-law slope correlation was not seen in L5TM steep and L5TM flat spectra. Depending on the amount and condition of some satellite images used in this study it can be stated that while L5TM instrument produced slopes too flat for even $-5/3$ power-law, the general correlation of ASAR and MERIS was fairly good for $-5/3$ and in some cases for -2 power-law slopes. It should also be pointed out that the power-law slopes used in this study were first characterized at pixel resolutions well above 10 km due to problems with the amount of data processing required.

6. SUMMARY AND CONCLUSION

By comparing L5TM, MERIS and ASAR instruments a rather ambiguous correlation was seen. For each of the instruments separately the spectra did not change much in their shape. The only exceptions were the small number of L5TM steep spectra, which produced significantly steeper spectra than L5TM flat. It was noted that as the scenes gained more resolution, the spectra started to get flatter. This possible connection however needs to be further investigated to determine if the decrease was caused by the resolution or rather the low sensitivity of L5TM's sensor and the different wavelength of ASAR.

MERIS spectral slopes followed a power-law slope of $-5/3$ (SQG theory) fairly well, where a mean slope of $-1,7$ to $-1,8$ was seen for both the Baltic Sea proper basin and the Gulf of Finland basin. In the wavenumber range 1-6 ASAR produced a mean slope of $-1,5$ where nearly half of the spectral slopes (6 out of 15) matched a power-law slope of $-5/3$. The scarce correlation that was found between submesoscale slopes and the well-known power-law slopes $-5/3$, -2 and -3 is arguably due to the difference in the process scale which they represent: well above 10 km, whereas in this study length scales of >10 km were investigated.

As this study was being conducted it was decided to also use a few clouded MERIS scenes and some of the less eventful scenes to see how their spectra differed from the cloud-free and more energetic MERIS scene spectra. The results showed that the actual spectra shape was quite similar between the more energetic image spectra and less energetic. Spectral slopes however showed significant differences, where inert water surface produced a shallower slope and clouded images produced slightly curved spectra.

REFERENCES

- Abraham, E. R., Law, C. S., Boyd, P.W., Lavender, S. J., Maldonado, M. T., Bowie, A. R. (2000). Importance of stirring in the development of an iron-fertilized phytoplankton bloom. *Nature* 407, 727-730.
- Alenius, P., Nekrasov, A., Myrberg, K. (2003). Variability of the baroclinic Rossby radius in the Gulf of Finland. *Continental Shelf Research* 23 (6), 563-573.
- AMORGOS 4.0p1. (2012). [WWW] <https://earth.esa.int/web/guest/-/amorgos-40p1-4410> (Accessed 29.04.2015)
- Anderson, M. (2012). A Faster Fourier Transform. *Technology Review* 115 (3), 41-43.
- Barsi, J. A., Hook, S. J., Schott, J. R., Raqueno, N. G., Markham, B.L. (2007). Landsat-5 Thematic Mapper Thermal Band Calibration Update. *Geoscience and Remote Sensing Letters* 4 (4), 552-555.
- Capet, X., McWilliams, J.C., Olemaker, M.J.M, Shchepetkin, A. F. (2008a). Mesoscale to Submesoscale Transition in the California Current System. Part I: Flow structure, Eddy Flux, and Observational Tests. *Journal of Physical Oceanography* 38 (1), 29-43.
- Capet, X., McWilliams, J.C., Olemaker, M.J.M, Shchepetkin, A. F. (2008b). Mesoscale to Submesoscale Transition in the California Current System. Part III: Energy Balance and Flux. *Journal of Physical Oceanography* 38 (10), 2256–2269.
- Charney, J. G. (1971). Geostrophic Turbulence. *Journal of the Atmospheric Sciences* 28 (6), 1087–1095.
- Chander, G., Markham, B. L., Barsi, J. A. (2007). Revised Landsat-5 Thematic Mapper Radiometric Calibration. *Geoscience and Remote Sensing Letters* 4 (3), 490- 494.
- Chu, E., George, A. (2000). INSIDE the FFT BLACK BOX: Serial and Parallel Fast Fourier Transform Algorithms. The United States of America: CRC Press LLC.
- Design. (2015). [WWW] https://earth.esa.int/web/guest/missions/esa-operational-eo-missions/envisat/instruments/asar/design#_56_INSTANCE_2sWV_matmp (Accessed 06.06.2015)

- Doney, S. C., Lima, I., Moore, J. K., Lindsay, K., Behrenfeld, M. J., Westberry, T. K., Mahowald, N., Glover, D. M., Takahashi, T. (2009). Skill metrics for confronting global upper ocean ecosystem-biogeochemistry models against field and remote sensing data. *Journal of Marine Systems* 76 (1-2), 95-112.
- Duhamel, P., Vetterli, M. (1990). Fast fourier transforms: a tutorial review and a state of the art. *Signal Processing* 19(4), 259-299.
- Eld, I. M., Pierrehumbert, R. T., Garner, S. T., Swanson, K. L. (1995). Surface quasi-geostrophic dynamics. *Journal of Fluid Mechanics*, 282, 1-20.
- ENVISAT Altimetry Level 2 User Manual. (2011). [WWW] <https://earth.esa.int/handbooks/> (Accessed 09.05.2015)
- European Space Agency. (2006). MERIS Product Handbook Issue 2.1. [WWW] <https://earth.esa.int/handbooks/> (Accessed 29.04.2015)
- Fennel, W., Seifert, T., Kayser, B. (1991). Rossby radii and phase speeds in the Baltic Sea. *Continental Shelf Research* 11 (1), 23-36.
- Ferrari, R., Wunsch, K. (2009). Ocean Circulation Kinetic Energy: Reservoirs, Sources, and Sinks. *Ann. Rev. Fl. Mech.* 41, 253-282.
- Friedrichs, M. A. M., Carr, M. E., Barber, R. T., Scardi, M., Antoine, D., Armstrong, R. A., Asanuma, I., Behrenfeld, M. J., Buitenhuis, E. T., Chai, F., Christian, J. R., Ciotti, A. M., Doney, S. C., Dowell, M., Dunne, J., Gentili, B., Gregg, W., Hoepffner, N., Ishizaka, J., Kameda, T., Lima, I., Marra, J., Mélin, F., Moore, J. K., Morel, A., O'Malley, R. T., O'Reilly, J., Saba, V. S., Schmeltz, M., Smyth, T. J., Tjiputra, T., Waters, K., Westberry, T. K., Winguth, A. (2009). Assessing the uncertainties of model estimates of primary productivity in the tropical Pacific Ocean. *Journal of Marine System* 76 (1-2), 113-133.
- Instruments. (2015). [WWW] <https://earth.esa.int/web/guest/missions/esa-operational-eo-missions/envisat/instruments> (Accessed 02.05.2015)
- Klein, P., Hua, B. L., Lapeyre, G., Capet, X., Gentil, S. L., Sasaki, H. (2008). Upper Ocean Turbulence from High-Resolution 3D Simulations. *Journal of Physical Oceanography* 38 (8), 1748-1763
- Klein, P., Lapeyre, G. (2009). The Oceanic Vertical Pump Induced by Mesoscale and Submesoscale Turbulence. *Annu. Rev. Mar. Sci.* 1:351–75, doi: 10.1146/annurev.marine.010908.163704

- Landsat 5 History. (2015). [WWW] http://landsat.usgs.gov/about_landsat5.php (Accessed 30.04.2015)
- Le Traon, P. Y., Klein, P., Hua, B. L., Dibarboure, G. (2008). Do altimeter wavenumber spectra agree with the Interior or Surface Quasigeostrophic theory? *Journal of Physical Oceanography*, 38 (5), 1137–1142.
- León, P., Blanco, J.M., Flexas, M.M., Gomis, D., Reul, A., Rodríguez, V., Jiménez-Gómez, F., Allen, J.T., Rodríguez, J. (2014). Surface mesoscale pico– nanoplankton patterns at the main fronts of the Alboran Sea. *Journal of Marine Systems* 143, 7-23.
- Leppäranta, M., Myrberg, K. (2009). *Physical Oceanography of the Baltic Sea*. Chichester, UK: Praxis publishing Ltd.
- Lévy, M., Ferrari, R., Franks, P. J. S., Martin, A.P., Rivière, P. (2012). Bringing physics to life at the submesoscale. *Geophysical Research Letter* 39(14), L14602, doi:10.1029/2012GL052756.
- Lévy, M., Klein, P. (2004). Does the low frequency variability of mesoscale dynamics explain a part of the phytoplankton and zooplankton spectral variability? *Proc. R. Soc. Lond. A* 2004 460, doi: 10.1098/rspa.2003.1219.
- Lévy, M., Klein, P., Treguier, A. M. (2001). Impact of sub-mesoscale physics on production and subduction of phytoplankton in an oligotrophic regime. *Journal of Marine Research* 59 (4), 535-565.
- Lévy, M., Resplandy, L., Klein, P., Capet, X., Iovino, D., Ethé, C. (2012). Grid degradation of submesoscale resolving ocean models: Benefits for offline passive tracer transport. *Ocean Modelling* 48, 1-9.
- Munk, W., Armi, L., Fischer, K., Zachariasen, F. (2000). Spirals on the sea. *Proceedings: Mathematical, Physical and Engineering Sciences* 456 (1997), 1217-1280.
- Osiński, R., Rak, D., Walczowski, W., Piechura, J. (2010). Baroclinic Rossby radius of deformation in the southern Baltic Sea. *Oceanologia* 52 (3), 417–429.
- Pavelson, J. (2005). *Mesoscale Physical Processes and the Related Impact on the Summer Nutrient Fields and Phytoplankton Blooms in the Western Gulf of Finland*. Tallinn University of Technology, Marine Systems Institute. [Doctoral thesis]. Tallinn.
- Qazi, W. A., Emery, W. J., Fox-Kemper, B. (2014). Computing Ocean Surface Currents Over the Coastal California Current System Using 30-Min-Lag Sequential SAR Images. *Geoscience and Remote Sensing* 52 (12), 7559-7579.

- Sasaki, H., Klein, P., Qiu, B., Sasai, Y. (2014). Impact of oceanic-scale interactions on the seasonal modulation of ocean dynamics by the atmosphere. *Nature Communications* 5, article 5636, doi:10.1038/ncomms6636.
- Stammer, D. 1997. Global characteristics of ocean variability estimated from regional TOPEX/ Poseidon altimeter measurements. *Journal of Physical Oceanography* 27, 1743–1769.
- VOLUME 8: ASAR PRODUCTS SPECIFICATIONS. (2012). [WWW] <https://earth.esa.int/web/guest/missions/esa-operational-eo-missions/envisat/instruments/asar> (Accessed 02.05.2015)
- The Thematic Mapper. (2015). [WWW] <http://landsat.gsfc.nasa.gov/?p=3229> (Accessed 02.05.2015)
- What is Envisat? (2015). [WWW] <https://earth.esa.int/web/guest/missions/esa-operational-eo-missions/envisat> (Accessed 29.04.2015)

Aknowledgements

The author of this bachelor`s thesis thanks Laura Raag from Marine Systems Institute for her guidance on satellite data processing.